Computational Modeling of Microfluid Devices with Free Surface Liquid Handling

H. Q. Yang and A. J. Przekwas
CFD Research Corporation
215 Wynn Drive
Huntsville, AL 35805
hqy@cfdrc.com, ajp@cfdrc.com
(205) 726-4824, 726-4815; Fax: (205) 726-4806

ABSTRACT

Integrated Microfluidic Systems are the subject of great scientific and commercial interest for a wide range of applications, including the biomedical, environmental, automotive, aerospace, and defense. This paper presents the computational methodology used in the ACE+MEMS CAD Software for design of fluidic devices incorporating free surface. The flow physics of the multi-fluid flow is solved with full Navier Stokes equations on 3-D unstructured grids. The unsteady motion of the free surface governed by the Hamilton-Jacobi evolution equation is solved on Eulerian grid using the Volume of Fluid (VOF) technique. Higher order surface reconstruction algorithms on unstructured grids are employed to predict the free surface shape. To predict the surface tension effects, the Laplace-Young high-order nonlinear boundary conditions at the liquid surface are needed to accurately model the liquid-gas interface and at the wall contact. For MEMS applications with a large aspect ratio geometry, the code allows mixed-dimensionality simulations in which 3-D domains are interfaced with 2-D channels. In reduced dimension channels, the Hele-Shaw model can be used for the free surface simulations. The paper presents basic mathematical formulation and numerical techniques used. The computational techniques and the software are validated/demonstrated on several MEMS microfluidic devices.

Keywords: CFD, Microfluidic, MEMS.

INTRODUCTION

Handling of fluids with liquid-gas interfaces in very small (micro) devices, such as channels, valves, pumps, mixers, separators, reactors, etc., poses several engineering and scientific challenges. One of the major design problems with microfluidic MEMS is to force the liquids into microchannels by proper application and control of two major forces: surface tension and externally applied pressure or vacuum. Depending on the wall surface physicochemistry, the fluid could impel (hydrophillic) or expel (hydrophobic) itself from channels. In very small channels (~1μm) the surface tension forces can be so large that even atmospheric-to-hand vacuum pressure differential force (14.7 psi) can not force the liquid into the channels. Computational modeling of this phenomena in MEMS has not been addressed yet.

On the other hand, using fluids in micro-electromechanical systems can increase electrical breakdown strength over a vacuum due to increased dielectric constant. This fluid can also act as a medium of power transmission, as in conventional fluid power systems, eliminating the need for complex mechanical transmissions. The unique feature of surface tension of the fluid provides a medium for bearings, unlike conventional viscosity. The surface tension of the liquid can be utilized in many microhydraulic actuators [Reference 1], as shown in Figure 1.

The purpose of this paper is to develop a computational methodology to model surface tension effects of multi-fluid flow in ACE+MEMS CAD software and to apply the technique to several practical microsystems.

COMPUTATIONAL FLUID DYNAMICS MODELING

The computational methodology used for simulation of the multi-fluid flow with surface tension is based on a Finite-Volume implementation of the SIMPLE (Semi-Implicit Pressure-Linked Equations) algorithm. The algorithm solves the continuity and momentum equations in the forms of:

$$\rho\frac{Du}{Dt} = -\frac{\partial p}{\partial x} + \mu\nabla^2 u + \rho f_x \tag{1}$$

$$\rho\frac{Dv}{Dt} = -\frac{\partial p}{\partial y} + \mu\nabla^2 v + \rho f_y \tag{2}$$

$$\rho\frac{Dw}{Dt} = -\frac{\partial p}{\partial z} + \mu\nabla^2 w + \rho f_z . \tag{3}$$

$$\frac{\partial \rho}{\partial t} + \rho\frac{\partial u}{\partial x} + \rho\frac{\partial v}{\partial y} + \rho\frac{\partial w}{\partial z} = 0 . \tag{4}$$

The solution procedure has been described in detail by Patankar [2].

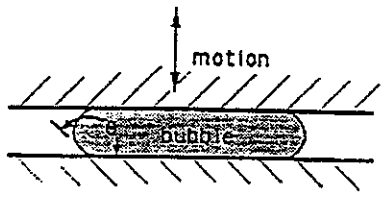

(a) surface tension bearing

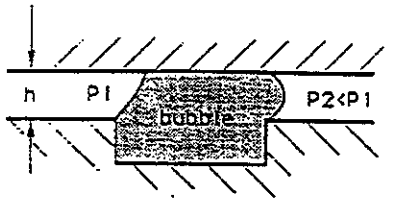

(b) surface tension seal

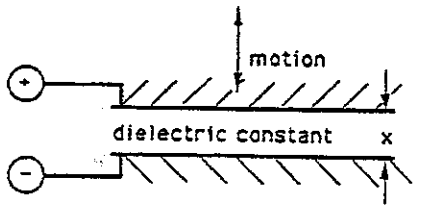

(c) variable-geometry capacitance normal motion

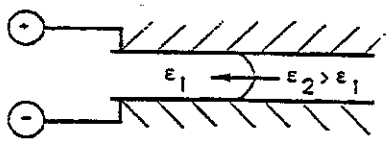

(d) EHD pumping of a meniscus

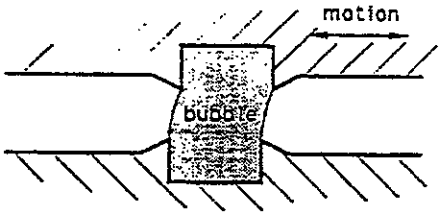

(e) surface tension with transverse motion

Figure 1. Primitive Functions Employing Fluids in Microsystems

VOF MODELING

The SIMPLE algorithm and its variants are particularly well-suited to the solution of steady, incompressible flow.

In multi-fluid flows, however, there is an additional requirement for the prediction of the location of the liquid front. This requires extension of the SIMPLE algorithm to two-phase flows. This extension was accomplished in this work by use of the Volume-of-Fluid (VOF) methodology, as first published by Hirt and Nichols [3] and recently extended by Rider and Kothe, et al [4].

The VOF scheme belongs to the family of volume tracking algorithms. The basic idea is to compute for each cell in the computational grid a scalar, F, which specifies the fraction of the cell's volume occupied by liquid. Thus, F takes the value 1 in cells which contain only liquid, the value 0 in cells which contain only gas, and a value between 0 and 1 in interface cells. Starting from an initial distribution of F at the start of a time-step, the total volume fluxes between cells are computed using the SIMPLE algorithm, which automatically takes into account the density distribution associated with the distribution of F across the grid. The proportion of liquid in the volume fluxes is determined and used to compute the net transfer of liquid into each cell, leading to the calculation of the final volume fraction of liquid throughout the computational domain at the end of the time-step. This procedure is repeated again for each time-step. From the mathematical point of view, the VOF technique is implemented within the framework of the SIMPLE algorithm by solving for the volume fraction in each cell as an additional scalar field variable that is convected with the fluid. The equation which is effectively solved in discrete form originates from the incompressible advection equation for F; namely:

$$\frac{\partial F}{\partial t} + u\frac{\partial F}{\partial x} + v\frac{\partial F}{\partial y} + w\frac{\partial F}{\partial z} = 0 \,. \qquad (5)$$

In addition to including F as another scalar variable, special modifications to the basic formulation in the SIMPLE algorithm are needed to enable the algorithm to robustly cope with the large density jumps that typically occur across liquid-gas interfaces.

Among the most important characteristics of the VOF scheme is its high efficiency and, being a volume tracking scheme, its ability to compute in a fully automatic manner flows where liquid masses coalesce, disintegrate, or undergo other arbitrary topologic transformations. These properties are the chief reasons for selecting this scheme for this application. On the other hand, compared to surface tracking schemes, the VOF scheme has the disadvantage of excessive

diffusivity, leading to smearing of interfaces across several cells. In order to counter this disadvantage, a higher-order surface reconstruction technique was implemented following the work of Rider and Kothe, et al [4] to better retain the sharpness of the discontinuous interface.

INTERFACE DYNAMICS AND SURFACE TENSION MODELING

Accurate modeling of interfacial flows requires high fidelity algorithms for the kinematics and dynamics of interfaces. In this study, we chose an Eulerian method to simulate flows with interfaces of arbitrarily complex topology. In an Eulerian method, the computational grid remains stationary, but interfaces are allowed to have arbitrarily complex shape. In addition, the interface dynamics, or those physics specific to the interface, must be modeled by local volumetric forces.

Assume that viscous effects are neglected at the free surface and assumed that the surface tension coefficient is constant, implying that the surface force has no tangential component. Then, the stress boundary condition reduces to Laplace's formula,

$$p_s \equiv p - p_v = \sigma\kappa \tag{6}$$

where the surface pressure, p_s, is the surface tension-induced pressure jump, p_v is the vapor pressure, and κ is the mean free-surface curvature, given by

$$\kappa = -(\nabla\cdot\hat{n}) = \frac{1}{|\vec{n}|}\left[\left(\frac{\vec{n}}{|\vec{n}|}\cdot\nabla\right)|\vec{n}| - (\nabla\cdot\vec{n})\right] \tag{7}$$

where the unit normal $\hat{n}$,

$$\hat{n} = \frac{\vec{n}}{|\vec{n}|}, \tag{8}$$

is derived from a normal vector $\vec{n}$, given by

$$\vec{n} = \nabla F, \tag{9}$$

where ∇F is the gradient of the VOF function. Because the curvature is proportional to the second derivative of the VOF function, surface force modeling is extraordinarily sensitive to small errors in the F distribution on the grid.

In this work, a conservative formulation for the calculation of surface tension forces was developed. This formulation is based on the equilibrium of a curved surface under a surface tension force, as shown in Figure 2.

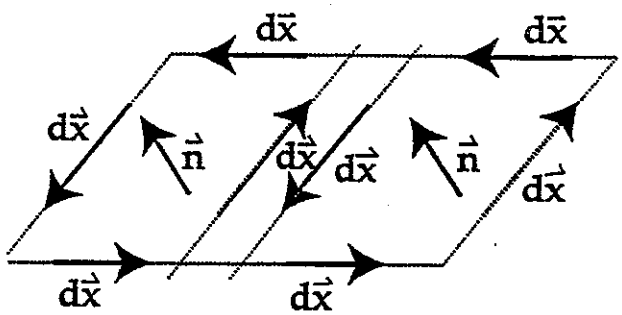

Figure 2. Equilibrium of a Free Surface Under Surface Tension

The net normal force acting on the surface should be equal to the summation of all the tangential force due to surface tension

$$\int \Delta p\, d\vec{s} = \int \vec{\tau}\,|d\vec{x}| \tag{10}$$

where the tangential force is equal to:

$$\vec{\tau} = \sigma\vec{n}x\frac{d\vec{x}}{|d\vec{x}|} \tag{11}$$

which leads to:

$$\int \Delta p\, d\vec{s} = \int \sigma\vec{n}x\, d\vec{x} \tag{12}$$

This formulation uses no information about the surface shape, and only the lines along the boundary of the surface are needed. When applied at the discrete level, the computation is conservative, in that when the interface is broken into many small pieces, the total force is equal to the summation of the forces over the constitutive pieces. Mathematically, it can be seen that due to the opposite traversal direction along an edge separating two cells, the contour integrals cancel except for the contributions from the outer boundary of the entire surface.

This formulation is implemented as follows:

1. Find the liquid-gas interface at each cell face (currently the isoline F = 0.5 is assumed).

2. Find the unit normal of the interface, based on $\vec{n} = \nabla\cdot F$.

3. Apply Equation (12) and find the net normal force and in turn use it as body force.

The above method has been found to be very successful.

VALIDATION STUDIES

Formation of Droplets and Bubbles

Here we consider a seemingly simple test, namely a static droplet in which the surface tension-induced pressure rise inside a 2D cylinder is computed and compared with the known analytical solution. The static droplet, presented in [5] as validation test of the original CSF model, has since been recognized as one of the most difficult tests for surface tension models based upon the Eulerian methodology. This is because of the difficulty of maintaining an equilibrium position for the droplet over many computational cycles. The computed pressure field inside the drop tends to have small numerical variations that induce artificial flows (recently dubbed "parasitic currents"), tend to grow in magnitude with each time step.

For a static droplet with surface tension acting along its interface with no gravity force, the pressure jump Δp across the droplet is given by

$$\Delta p = \sigma\kappa, \tag{13}$$

where κ is the droplet curvature, equal to 1/R in 2-D and 2/R in 3-D, and σ is the surface tension coefficient. The theoretical surface tension-induced droplet pressure difference is

$$\Delta P_{theory} = \begin{cases} \sigma/R & in\ 2D \\ 2\sigma/R & in\ 3D \end{cases}. \tag{14}$$

Our initial condition is such that the pressure is zero everywhere, and if the center of any control volume falls within a radius of R, the F will be initialized to 1, i.e., the cell will be filled with liquid. The density ratio between the liquid and gas is 10^3. Due to surface tension, the pressure will build up within the liquid, as given by Equation (13).

The computational grid and initial conditions are shown in Figure 3. The solutions are also given in this figure. The pressure rise is in excellent agreement with the analytical solution.

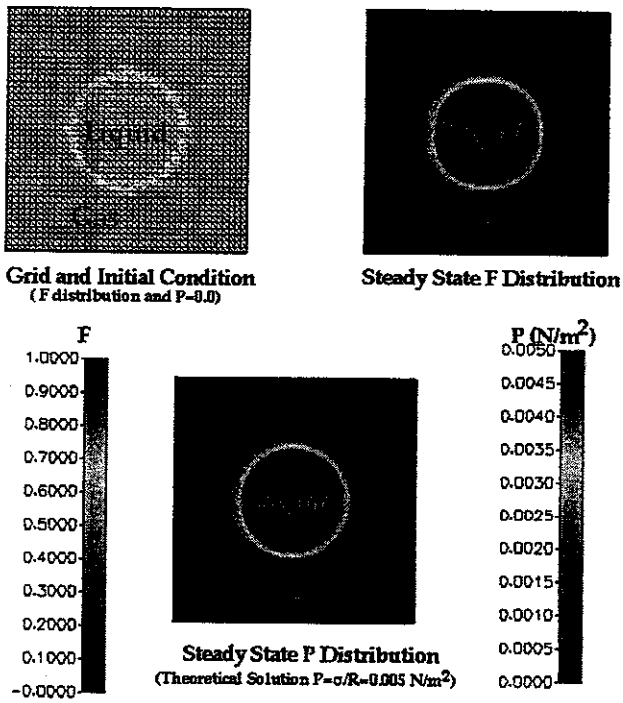

Figure 3. Validation for a Liquid Droplet in the Gas Under Surface Tension Force

Liquid Flow in a Channel

If we ignore the effect of surface roughness, flux residues, and flow obstructions, and assume an infinite supply of liquid without end effects, we can derive an analytical solution for the propagations of a liquid in a channel. This analytical solution is based on the Navier-Stokes equation for incompressible, quasi-steady, laminar, Newtonian 2D horizontal flow,

$$-\frac{\partial p}{\partial x} = -\mu\frac{\partial^2 V_x}{\partial y^2} \tag{15}$$

where p is the pressure in the fluid at x, μ is the viscosity of the fluid, V_x is the velocity of the fluid, and the coordinates x and y are oriented as shown in Figure 4. Since each side of (15) is independent of the other, the partial differential equation can be separated into two ordinary different equations

$$\frac{dp}{dx} = -\beta \tag{16}$$

$$\mu \frac{d^2 V_x}{dy^2} = -\beta \qquad (17)$$

where β is a constant.

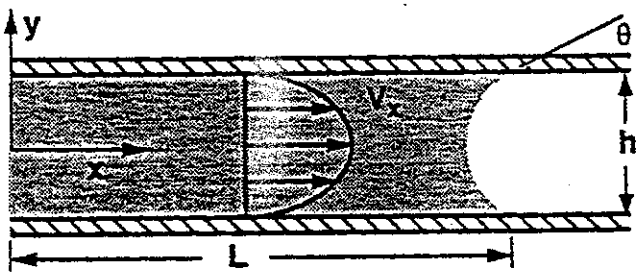

Figure 4. Flow Between Parallel Plates

By applying appropriate boundary conditions, the advancements of the front into the channel is found to be given by:

$$L = \left(\frac{ht\sigma\cos\theta}{3\mu} \right)^{1/2} \qquad (18)$$

or

$$t = \frac{3\mu L^2}{h\sigma\cos\theta} . \qquad (19)$$

Equation (18) and (19) show that the flow time is inversely proportional to the surface tension, separation distance, and the cosine of the wetting angle, and directly proportional to the viscosity and the square of the flow distance.

To compare with the above analytical solution, our computational model is shown in Figure 5. The channel height is h = 0.125 mm, the total length is L = 1.875 mm, the surface tension coefficient is 15×10^{-3} N/m, and the liquid viscosity is $\nu = 0.78 \times 10^{-3}$ m^2/sec.

Figure 6 shows the front propagation under the capillary force. It can be seen that velocity is rather high initially and starts to decrease. Our prediction shows a very sharp front. The pressure distribution is given in Figure 7.

Since the driving force is constant at $2\sigma/d$, the initial pressure gradient is relatively high. As time progresses, the pressure gradient becomes smaller, hence the front moves slower. The front position as a function of time is shown in Figure 8, and we see very good agreement with analytical solution.

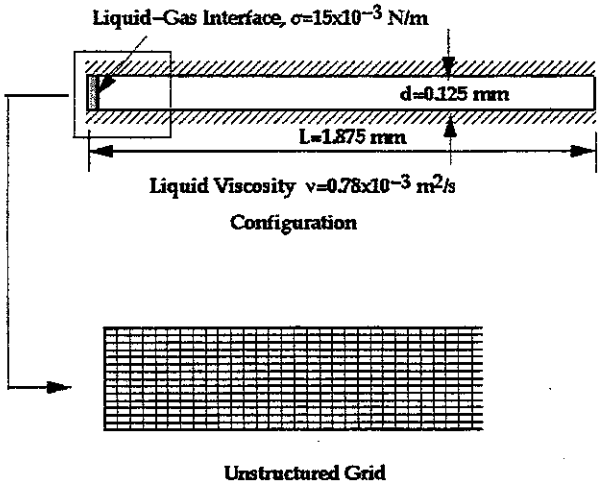

Figure 5. Configuration of Surface Tension Flow in a Channel

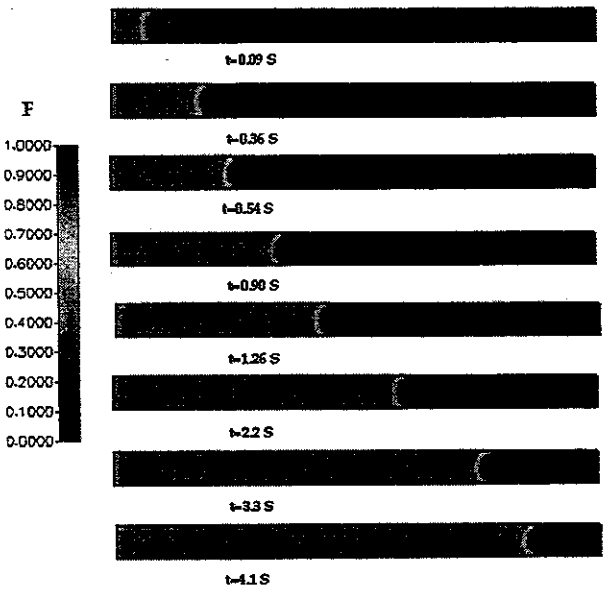

Figure 6. Liquid-Gas Front Propagation in a Channel Due to Surface Tension

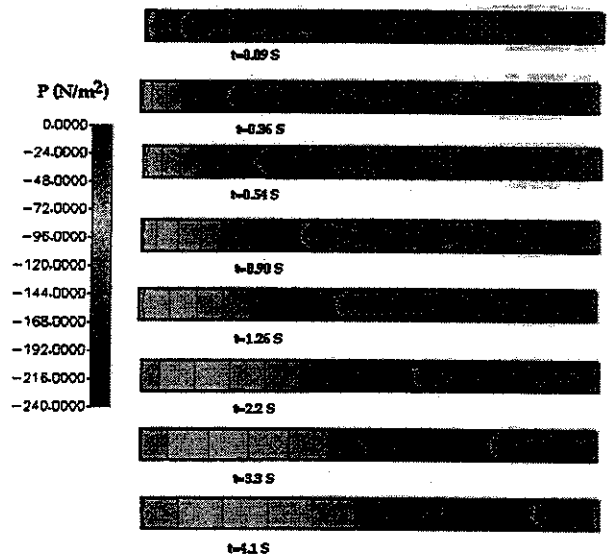

Figure 7. Pressure Distribution in a Channel Due to Surface Tension

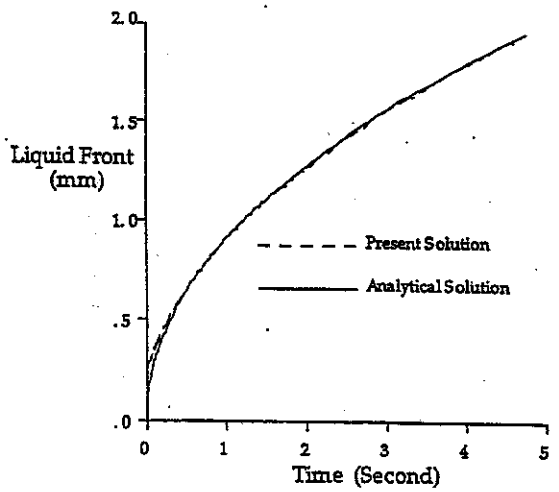

Figure 8. Comparison Against Analytical Solution

RESULTS

Next, we will show some applications of the present model to microfluidic.

Liquid Transport in Microchannels

Here, we study fluid flow in extremely small channels. The potential applications for such channel include cooling of electronic circuits, and reactors for modification and separation of biological cells. In the manufacture process, the liquid should enter the channel through one or more ports that likely must be sealed off subsequently. Two forces are available to induce the transfer: surface tension and an externally applied pressure or vacuum. In the above demonstration case, the externally applied force does not exist, and the transport is due to surface tension. It is true only when contact angle is less than 90°. On the other hand, with a contact angle greater than 90°, the fluid must be pressurized to induce transport. The pressure force has to be higher than the pressure jump across the interface. Actually, Pfahler et al [6] have reported that 0.5 μm channels blocked for water flow, and Stemme [7] found three times higher flow of alcohol than water through a 0.2 μm filter.

The numerical model of liquid transport in a microchannel is shown in Figure 9. Here the liquid properties are the same as Figure 5, but the channel height has been reduced to 1.25 μm. The case (a) and (b) corresponds to vacuum transport. Two extreme contact angles are presented: (a) $\alpha = 0°$ and (b) $\alpha = 180°$. The front shape can be seen to be very different. At $\alpha = 0°$, the surface tension assists the flow whereas $\alpha = 180°$, the surface tension force resists the motion. As a result, one sees slower transport of the front. For comparison purpose, Figure 9(c) shows the front due to surface tension driven alone. The liquid front positions with time again are shown in Figure 10. Due to the fact that the driving force is constant, the front position is proportional to the square root of time, as explained above.

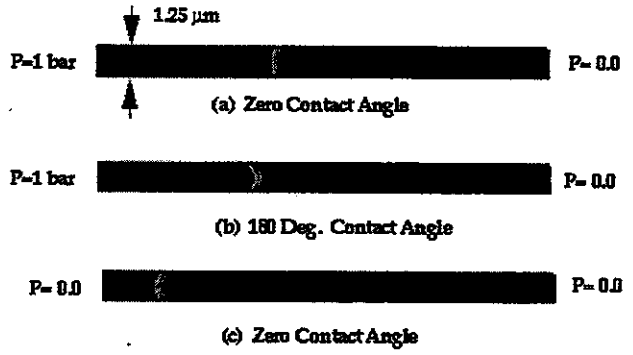

Figure 9. Surface Tension Effect on Liquid Flow in a Micro-Channel

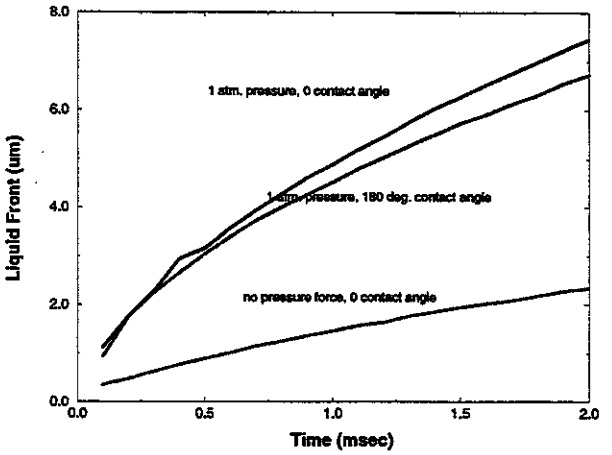

Figure 10. Liquid Front Propagation Due to Under Pressure and Surface Tension Forces

Figure 11 shows the transport of liquid in a multi-channel.

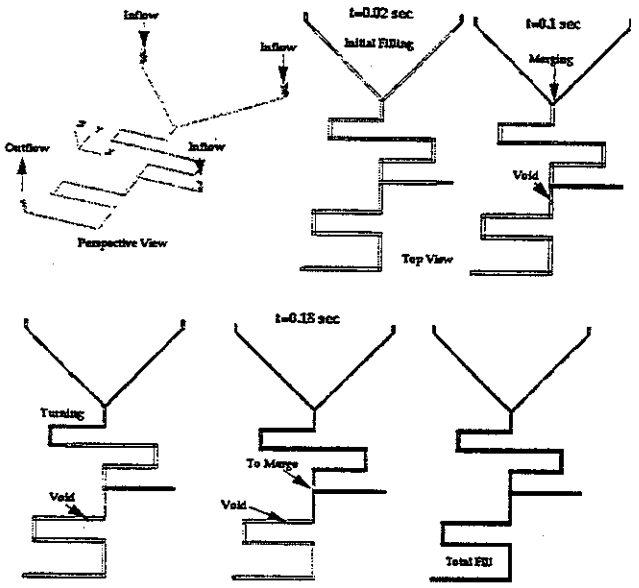

Figure 11. Liquid Filling of a Micro-Channel Using ACE+MEMS Model

Bubble Valve

Surface tension can be further utilized as check valves. The functio of the valves is shown in Figure 12. Here the bubble can b a gas, liquid-mercury, or gallium. The bubble is a perfect circle when there is no pressure drop in either direction. In the design, the bubble just graces the sealing corner. The corner is placed such that the directions of the forces which can be exerted on the bubble from the two channels are normal to each other. In Figure 12(a), when the pressure is high on the left side, the bubble is pushed into the right channel, producing a pressure drop across the free face. This pressure drop counts against supplied pressure to prevent the flow. In Figure 12(b), when the pressure is high on the right side, the valve opens up and functions as conducting the fluid in the leftward direction. The present model accurately predicts the above phenomena.

Pumping in Microchannel

Surface tension can also be used to pump flow motion in a microchannel. This pumping mechanism is achieved by using the property of variation of surface tension with temperature, and it requires no mechanical moving parts for actuation.

The operating mechanism of the micropump is shown in Figure 13. The relevant forces acting on the vapor bubble include vapor pressure, surface tension, and momentum due to evaporating and condensation.

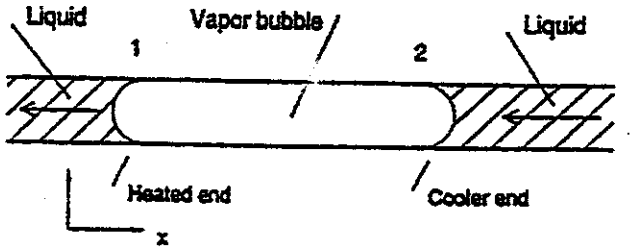

Figure 13. Micropump Mechanism by Heating a Bubble in a Microchannel

At uniform temperatures, as long as gas bubble completely covers the cross section area of the channel, there will be no net surface tension force. However, once the bubbles is asymmetrically heated, the surface tension will decrease with increasing temperature, resulting in a net force directed toward to higher temperature point. This force will produce a motion in the channel. Jan and Kim [8] has investigated the feasibility of pumping fluids in a 3.4 μm hydraulic diameter microchannel using asymmetric heating and transferring bubbles. Their results revealed that variations in vapor pressure and surface tension (marangoni effect) are the two dominant forces.

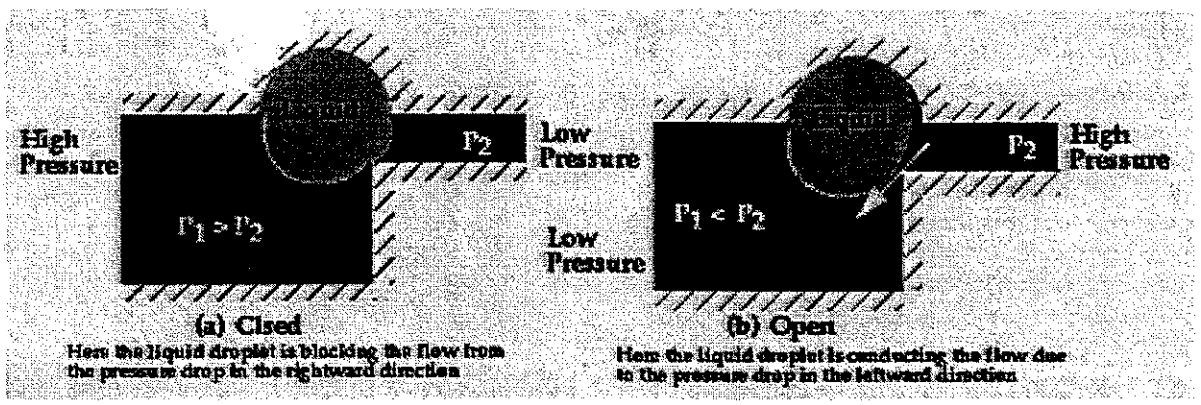

Figure 12. Computational Simulation of a Microfluidic Bubble Check Valve

Our Computational model and results are shown in Figure 14. Here the heating is assumed to be linear along the length and the surface tension is a linear function of temperature. The transport of the bubble is clearly seen. The pressure distribution in and around the bubble reveals that there is a pressure gradient across the bubble which drives the flow.

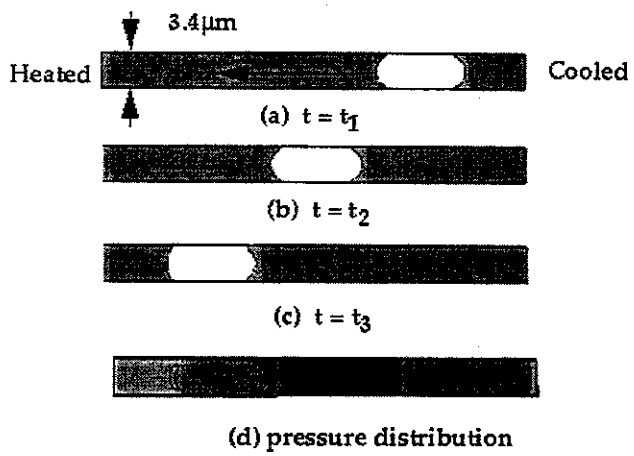

Figure 14. Transportation of Gas Bubble Under Asymmetric Heating

SUMMARY

This paper presents a high-fidelity numerical simulation tool for liquids in micro-devices. On of the important problems is the modeling of surface tension effect. To this end, a innovative conservative algorithm for surface tension force is developed, which is shown to have high numerical stability, and to accurately predict the correct transport speed of the liquid front.

Systematic validations were made whenever possible again analytical solutions. All of our results have shown excellent agreement. The developed model has also been applied to several MEMS devices: liquid-filling in microchannel with hydrophillic and hydrophobic surfaces, liquid filling of multi-channels, and bubble check valve. Extension to variable surface tension is also shown for the problem of microscale pumping.

ACKNOWLEDGMENTS

The work presented here is partially funded by DARPA and the Plastic Packaging Consortium under contract number RSC680512. The authors would like to thank Dr. Luu Nguyen of National Semiconductor, Dr. Dan Radack of DARPA/ETO, and Dr. Nick Naclerio (formerly at DARPA/ETO) for their technical and financial support. Helpful technical contributions from Drs. Samuel Lowry, Sami Bayyuk, and Anantha Krishnan of CFD Research Corporation are also greatly appreciated.

REFERENCES

[1] Brown, F.T., "Potential Building Blocks for MicroHydraulic Actuators," DSC vol 40, Micromechanical Systems, ASME, pp. 21-33, 1993.

[2] Patankar, S., Numerical Heat Transfer and Fluid Flow, Hemisphere Publishing Corp., New York: McGraw Hill, 1980.

[3] Hirt, C.. and Nichols, B., "Volume of Fluid (VOF) Method for the Dynamics of Free Boundaries," *J. Comp. Physics*, vol. 39, pp. 201-225, 1981.

[4] Rider, W.J., Kothe, D.B., Mosso, S.J., Cerutti, J.H., and Hochstein, J.I., "Accurate Solution Algorithms for Incompressible Multiphase Flows," AIAA-95-0699, 1995.

[5] Kothe, D.B. and Mjolsness, "RIPPLE: A New Model for Incompressible Flows with Free Surfaces," *AIAA Journal*, vol. 30, pp. 2694-2700, 1992.

[6] Pfahler, J., Harley, J., Bau, H., and Zemel, J., "Liquid Transport in Micron and Submicron Channels," *Sensors Actuators*, A 21-23, 431-4, 1990.

[7] Stemme, G., Kittilsland, G., and Norden, B., "A Submicron Particle Filter in Silicon," *Sensors Actuators*, A 21-23 907-7, 1990.

[8] Jun, T.K. and Kim, C.J., "Micro-scale Pumping with Traversing Bubble in Microchannels," Solid State Sensor and Actuator Workshop, Hilton Head, South Carolina, pp. 144-147, June 2-6, 1996.